Photon-Induced Near-Field Electron Microscopy of Nanostructured Metallic Films and Membranes

Sophie Meuret, Hugo Lourenço-Martins, Sébastien J. Weber, Florent Houdellier, Arnaud Arbouet

Photon induced near-field electron microscopy of nanostructured metallic films and membranes

Sophie Meuret,* Hugo Lourenço-Martins, Sébastien Weber, Florent Houdellier, and Arnaud Arbouet*

CEMES-CNRS, Université de Toulouse, CNRS, Toulouse, France

E-mail: sophie.meuret@cemes.fr; arnaud.arbouet@cemes.fr

Abstract

We investigate - both experimentally and theoretically - the inelastic interaction between fast electrons and the electromagnetic field scattered by metallic apertures and nanostructures on dielectric membranes using photon induced near-field electron microscopy. The experiments - performed in a high brightness ultrafast transmission electron microscope - on gold apertures on silicon nitride membranes reveal strong modulations of the electron-light coupling strength. We demonstrate that this effect results from the combined action of the electric field scattered by the aperture edges and the reflection and transmission of the incident wave by the dielectric membrane. Moreover, when a nanostructure is added inside the metallic aperture, the new scattered field interferes with the previous contributions, thus imprinting the optical response of the nanostructure in additional modulations of the electron-light coupling strength. Using systematic electrodynamics simulations based on the Green dyadic method, we quantitatively analyze these different contributions to the electron-light coupling and propose further applications.

Introduction

Ultrafast Transmission Electron Microscopes (UTEM) combining the femtosecond temporal resolution of ultrafast optical spectroscopies and the nanometric spatial resolution of electron microscopy have opened up many new possibilities to study the ultrafast dynamics and optical response of materials at unique spatio-temporal scales[1,2]. Their development has already had a major impact on several fields of nanosciences such as nano-optics, nanomechanics[3] or nanomagnetism[4] and detailed reports of the progress made in this rapidly evolving field can be found in several review articles[1,2,5,6]. Photon-Induced Near-field Electron Microscopy (PINEM) is one of the most impactful electron based spectroscopy techniques enabled by UTEMs. It exploits the inelastic coupling between the fast electrons and an optically excited nanostructure[7–9]. In the latter, the inelastic interaction between the fast electron and the electromagnetic field results in multiple exchanges of light quanta by the moving charge with a probability that depends on the strength of the electric field at the position of the electron beam[7,10]. The quantitative analysis of the electron energy spectrum after interaction therefore enables the mapping of the electric field at metallic interfaces or the study of the optical modes of photonic or plasmonic nanostructures and nanoparticles[11–13]. Furthermore, the coherence of the interaction between electrons and light allows more sophisticated schemes involving multiple interactions of the electron with phase-locked optical pulses to coherently control the free electron wavefunction[14–17].

In this context, the use of dielectric membranes has several advantages for the implementation of coherent control schemes. Contrary to the case of nano-objects that yield strongly inhomogeneous evanescent fields, the electric field strength at planar interfaces is homogeneous on the entire electron beam cross-section. Furthermore, it is possible to adjust the membrane tilt angle so that each part of the electron beam interacts with the same optical phase[18]. These assets have been used for instance to coherently manipulate on the attosecond timescale the free-electron wave function using pairs of light pulses reflected from a mirror[19].

Recently, it has been proposed to exploit the inelastic interactions of fast electrons with a tailored light beam reflected by a dielectric membrane to correct the spherical aberration of electron microscopes[20]. In a first proof-of-principle experiment in this direction, the electron-light coupling mediated by a dielectric membrane illuminated by a tilted plane wave has been exploited to imprint different transverse intensity profiles on the electron wave function[21]. The interaction of a tilted plane wave with a dielectric membrane or metallic mirror can also be used in so-called holographic PINEM experiments. While conventional PINEM experiments give access to the optical-near field intensity along the electron trajectory, holographic PINEM experiments detect the interference of the studied optical excitation with a reference wave generated e.g. by a reflection of the incident wave by a planar interface. It has been shown that such interference between the plasmon field excited at a metal/dielectric interface and the reflection from the sample can imprint the phase of the plasmon field in the electron/near-field coupling constant extracted from the PINEM signal[22]. Holographic PINEM experiments have also been performed in a different geometry involving two sequential inelastic interactions induced by two distinct samples placed at different locations along the electron beam trajectory[14]. Even though the presence of a membrane in electron spectroscopy experiments is unavoidable, its has been shown that it is possible to minimize its influence on the electron-light coupling by choosing the incidence angle so that the contributions from the incident and reflected electric fields almost completely cancel each other[19]. This is however not always possible in particular when the space available in the objective lens of the microscope is very limited or when short focal distance focusing optics are used on the sample. In these latter cases, a detailed knowledge of the contribution from the membrane to the inelastic signal is required prior to any demanding PINEM experiment.

In this study, we investigate both experimentally and theoretically the inelastic interaction between fast electrons and the electromagnetic field scattered by metallic apertures and nanostructures fabricated on a dielectric membrane (see Figure 1). Using Photon Induced Near-field Electron Microscopy (PINEM), we map the inelastic interaction probability and

analyze the combined influence of the light scattering by the aperture edges or nanostructures and the electric field reflected or transmitted by the dielectric membrane illuminated by a tilted plane wave on the electron-light coupling. We have performed two sets of experiments on apertures and nano-antennas engraved in a 50 nm gold film with a focused ion beam (See SI). The gold film is deposited on a silicon nitride membrane. First, we have investigated the spatial distribution of the inelastic signal when the fast electrons travel through simple apertures of different shapes then we considered the case in which a gold nanostructure stands in the middle of the aperture. The results of the PINEM experiments are analyzed using electrodynamical simulations based on the Green dyadic Method.

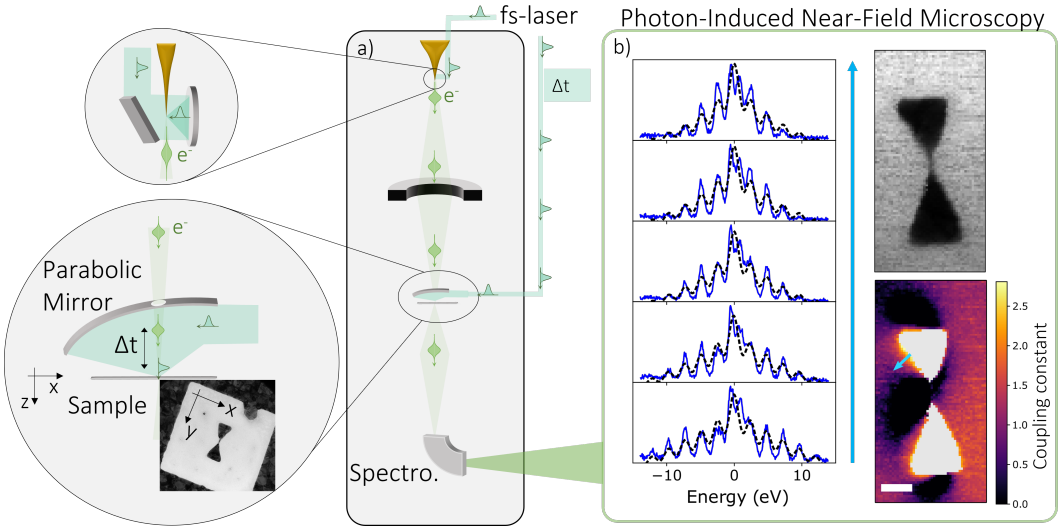

Fig. 1: (Color Online) a) Photon-Induced Near-field Electron Microscopy. The excitation laser pulse is focused on the sample by a parabolic mirror (incidence angle $\theta_i = 35°$). The electron and laser pulses are synchronized by a delay line (not shown) and the energy spectrum of the electron pulse is analyzed by an electron spectrometer after interaction with the optical pulse. Inset: Bright field image of the sample recorded with a continuous electron beam. b) Electron energy spectra (solid line) and fit (dashed lines) recorded at different positions along the arrow. Right Top : Bright field image recorded at the same time as the electron energy spectrum. Right bottom: Map of the electron-light coupling constant (g) extracted from a fit of the electron energy spectra acquired at each pixel. Scale bar : 200 nm

Inelastic electron-light interactions in apertured metallic films

PINEM works on a so-called pump-probe scheme: A first laser pulse (pump) excites the optical near-field around a nanostructure which is then probed by a subsequent electron pulse (probe). During its transit in the optical near-field, the travelling electron can emit or absorb photons, thus leading to a modification of its energy. This inelastic interaction yields a characteristic electron energy spectrum composed of a series of peaks reflecting the discrete nature of the photon exchange. The magnitude of these peaks only depends on the so-called electron-light coupling strength g which is proportional to the Fourier transform of the electric field component along the electron trajectory[7,9,10]:

$$g = \frac{e}{2\hbar\omega} \int dz \; E_z(z) e^{-\imath\omega z/v} \tag{1}$$

After interaction, the exit wavefunction of the electron, initially having an energy E_0, is a superposition of wavelets of different kinetic energies $E_n = E_0 + n\hbar\omega$. The amplitude of the different components is a function of the electron-light coupling constant g.

The PINEM experiments have been performed on the high-brightness ultrafast TEM developed in CEMES-CNRS. The latter is a customized 200 kV cold-field emission Hitachi High-Technology HF2000[23]. The electron gun has been modified so that femtosecond laser pulses can be focused onto the tungsten nanotip and trigger the emission of femtosecond electron pulses[24]. The high brightness of the femtosecond electron source provides sub-400 fs electron pulses that can be focused in spots as small as 1 nm on the sample. The electron microscope has been modified to allow optical excitation of the sample inside the objective lens. A high numerical aperture parabolic mirror with XYZ translation stage has been added between the objective lens pole pieces yielding a tilt angle of 35° between the electron probe and the optical pump focused on the sample (see Figure 1). Both the electron emission and

excitation of the sample are achieved using the 515 nm second harmonic of an ytterbium-doped fiber laser (Amplitude Satsuma, 1030 nm, 2 MHz, 250 fs). The average power incident on the sample typically lies in the 20-30 mW range. Figure 1-b shows an example of the nanostructures investigated by PINEM in this study. These structures are nano-antennas within a 1.1 μm square aperture fabricated from a 40 nm thick gold film evaporated on a 50 nm thick Si_3N_4 membrane (see the Supplementary Information for more details). At each point of the map, an electron energy spectrum such as the ones shown in Figure 1-b is acquired with a Gatan PEELS 666 with a typical integration time between 300 and 500 ms/pixel. The collection of energy spectra is then post-processed to extract the electron-light coupling constant at each point of the map (see the Supplementary Information for more details about PINEM theory and data processing). In the experiments reported in this study, the electron beam is accelerated at 150 keV. The ultrafast TEM is operated close to the single electron regime with electron pulses each comprising 1-10 electrons. As discussed in a previous publication, even in this regime the electron pulse has a non-negligible chirp which strongly depends on the number of electrons per pulse and causes the splitting of the zero loss peak visible on the spectra displayed in Figure 1-b[25]. Even if this phenomenon is very well understood and accurately simulated it makes it very difficult to extract from the fit an accurate value of the coupling constant g. The g maps displayed in Figures 1, 2 and 3 used a fit routine detailed in the SI. Although the routine nicely reproduces the shape of the experimental spectrum and provides g values having the correct order of magnitude, the estimated precision is rather low. The supplementary material provides more details about the fitting procedure and influence of the splitting of the zero loss peak. The use of a 30 μm STEM aperture allows to focus the electron probe in a few nm spot[23,25]. The electron is travelling along the (Oz) axis, perpendicular to the (OXY) plane of the membrane. The position of the electron beam on the membrane is identified by the coordinates x and y. The (Ox) axis lies in the plane of incidence whereas the (Oy) axis is perpendicular to the latter (see Figure 1).

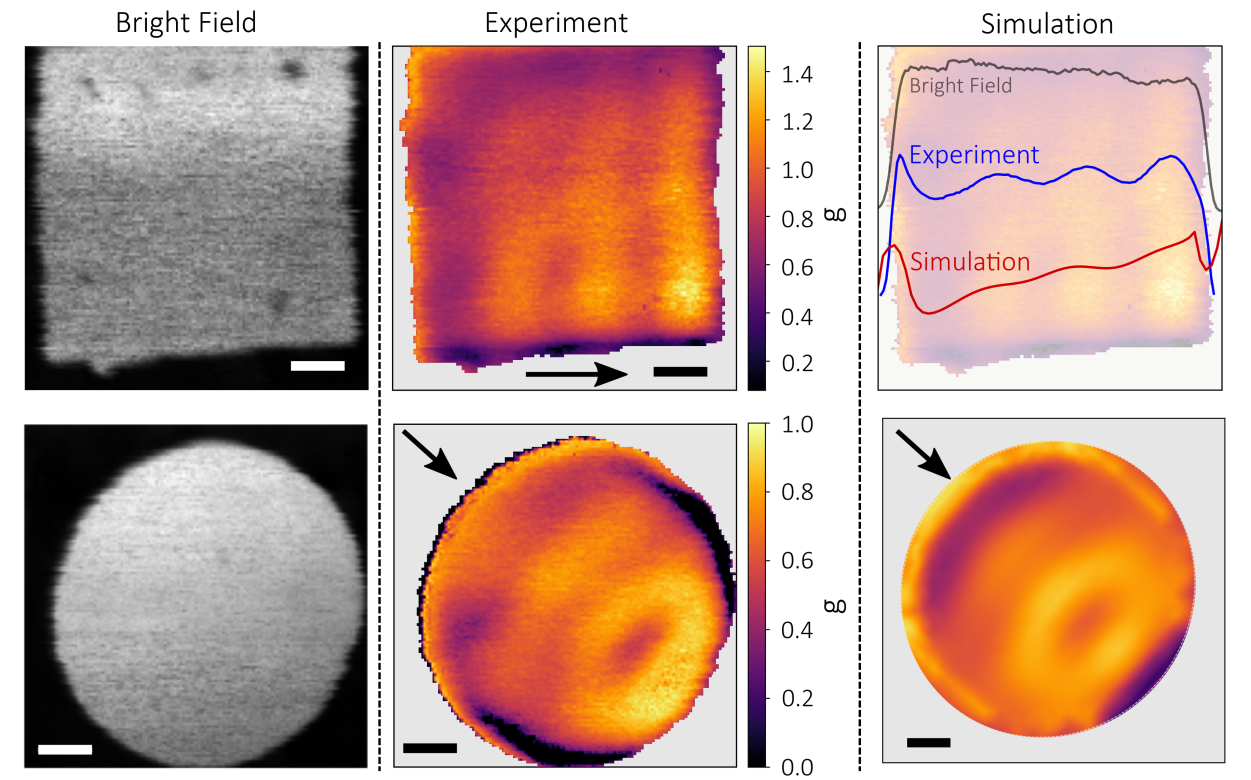

Fig. 2: (Color Online) Map of the electron-light coupling strength on an apertured gold film deposited on a silicon nitride membrane. Bright field image of respectively a square (top) and a circle (bottom) aperture fabricated in a 40 nm thick gold film deposited on a 50 nm thick Si_3N_4 membrane. Experiment : Map of the electron-light coupling strength g extracted from numerical fits of the electron energy spectra for the square (top) and circle (bottom) aperture. Simulation: Electron-light coupling constant computed from electrodynamical simulations based on the Green Dyadic Method. Top : Overlay on top of the experimental data, a comparison of the simulation (red line) and experiment (dark blue line), the gray line represent the bright field intensity profile). Bottom : 2D simulation map in the case of the circle aperture. For each panel, the scale bar is 200 nm and the black arrow represents the direction of the light.

In a first set of experiments, we study the electron energy exchanges when the fast electrons travel through apertures of different shapes. The spatial variations of the electron-light coupling constant g extracted from the PINEM maps acquired on square and circular apertures are shown in Figure 2. Clear modulations of g are visible in the apertures.

The origin of these modulations can be traced back from the definition of the coupling constant g (Equ. (1)) that governs the electron-light interaction probability. In vacuum, the momentum mismatch between light in free space and the moving electron leads to a vanishing g and therefore no interaction. Additional data acquired on similar apertures without the silicon nitride membrane confirm that there is no detectable inelastic signal at the center of the aperture (data available in SI). On the opposite, in the presence of a membrane, the coupling between the electron and the electromagnetic field is possible and the inelastic interaction probability depends on the wavelength, the intensity and the angle of incidence of the incident wave, as well as the membrane dielectric constant[19]. Taking into account the multiple reflections at the two vacuum/membrane interfaces, g_{mem} can be written as:

$$g_{mem} = \frac{\imath\, e}{2\hbar\omega} e^{\imath k_{i,x}.x} f(\omega, \theta_i, n_m, v, d) \tag{2}$$

in which f is a complex function of the angular frequency of light ω, the electron speed v, the membrane refractive index n_m and thickness d and the incidence angle θ_i. The complete expression of g_{mem} taking into account the multiple reflections at the two vacuum/membrane interfaces is given in supplementary information. It is clear from equation (2) that the modulus of g_{mem} on a simple membrane is not expected to display any spatial modulation.

The spatial modulations of the electron-light coupling strength visible in Figure (2) may arise from the combined influence of (i) the contrast in reflectivities between the metal and the dielectric surface and (ii) the scattering from the film edge. First, the existence of a separation between two regions of different reflectivities in the sample plane makes the

moving charge interact with the electric field reflected either by the gold surface or by the silicon nitride membrane depending on the distance between the electron and the membrane. The transition between the two cases does not occur for the same value of z depending on the distance of the electron beam to the aperture edge. The expression of the electron-light coupling strength resulting solely from the difference in reflectivities predicted by a simple model in the geometrical approximation can be found in the SI. This model predicts a spatial modulation of the electron-light coupling strength in poor agreement with the experiment. The origin of the discrepancy lies in the fact that a crude geometrical approach neglects the important contribution of the wave scattered by the film edge. For p-polarized illumination, the scattering by the film edge yields an electric field having a z-component comparable to the incident wave and therefore a significant contribution to the electron-light coupling. The latter is expected for p-polarized illumination to contribute to the electric field along the electron trajectory. The electric field scattered by the metallic film edge predicted by the Sommerfeld model is shown in Figure 3-b[26].

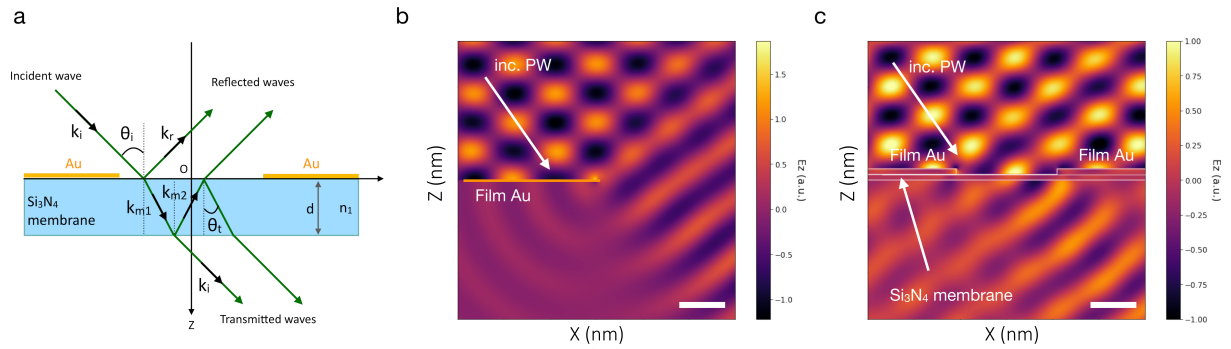

Fig. 3: (Color Online) a) Sketch of the experiment showing the beams reflected and transmitted by the membrane. b) Component along the electron trajectory of the electric field scattered by a semi-infinite half plane as predicted by the Sommerfeld model. c) Total electric field on the sample computed from 2D electrodynamical simulations based on the Green Dyadic Method. Scale bar = 500 nm

To take into account the different contributions discussed above, we have performed electrodynamical simulations using the Green Dyadic Method (GDM)[27,28]. We have used the

pyGDM open-source python toolkit[29]. pyGDM relies on the concept of a generalized propagator and allows to perform electro-dynamical simulations giving access to a large variety of near-field or far-field optical properties of individual nano-structures under either optical or electronic excitation[30]. More details about the GDM simulations are provided in the supplementary information. The influence of the scattering by the metallic film edge and the difference in reflectivities from the gold film and silicon nitride membrane have first been simulated using 2D GDM simulations considering a silicon membrane half covered by a gold film. We have plotted in Figure 2) the electron-light coupling strength computed using 2D-GDM across a 1100 nm gap made in a gold film deposited on a silicon nitride membrane. The results of the 2D-GDM calculations are in good agreement with the profile extracted from the experimental data acquired on the square aperture. We show in Figure 3-c the total electric field on the sample computed using 2D-GDM. A detailed study of the different contributions to the spatial variations of the electron-light coupling constant (see supplementary information) shows that scattering by the aperture edges and the reflection/transmission by the dielectric membrane contribute in comparable proportions to the modulation of the inelastic interaction strength. The case of more complex in-plane shapes requires full 3D electrodynamical simulations. Figure 2 shows the results of 3D-GDM calculations performed on the circular aperture. Again, a good agreement is obtained between the experiment and the electrodynamical calculations.

In a second set of experiments, we have studied the electron-light coupling strength on apertured metallic films in which a nanostructure has been added on the silicon nitride membrane in the square apertures. As shown in Figure 4, the sample consists of a square aperture with a bowtie antenna made of two equilateral gold prisms with an edge length $e = 200$ nm located at the center of the aperture. The exact same geometry has been fabricated several times with varying orientations with respect to the optical excitation. Figure 4 shows the bright field images and maps of the electron-light coupling strength

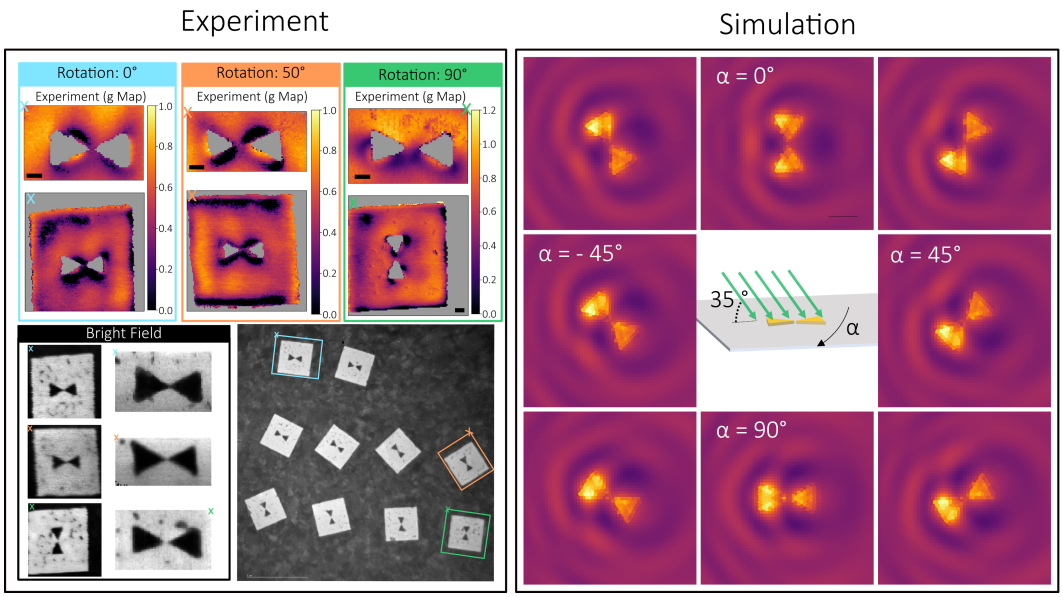

Fig. 4: (Color Online) Experiment: Top) PINEM maps of the electron-light coupling constant $|g|$ acquired on 3 different apertures with different orientations with respect to the illumination. Scale bar : 100 nm. Bottom) Bright field image of the studied sample. Simulation : Maps of the electron-light coupling constant $|g|$ computed using 3D-GDM simulations on a gold bow-tie (200 nm edge length, 160 nm gap) placed in on a silicon nitride membrane.

extracted from the electron energy spectra acquired at each position. Away from the bowtie antenna, the spatial distribution of the inelastic interaction strength is very similar to the case of the empty aperture. Closer to the nano-antenna, the interaction strength shows complex spatial variations with both regions in which the presence of the nano-antenna reinforces the coupling strength and regions in which the latter is diminished with respect to the case of the empty aperture. To analyze these observations, we have performed 3D-GDM simulations considering a gold bowtie on a silicon nitride membrane. The results are displayed in Figure 4. In the near-field region, the optical near-field includes large wavevector components that couple efficiently with the moving electron. When the orientation of the particle with respect to the plane of incidence is changed, the regions where the electron couples efficiently to the electron are also modified, following the topography of the optical near-field of the nano-antenna. The electron-light coupling does not vanish away from the antenna as the dielectric contrast at the surface of the substrate mediates the coupling between the incident wave and the moving charge. The situation would be different for a gold nano-antenna placed in

vacuum : the electron-light coupling would vanish outside of the near-field zone due to the momentum mismatch between the fast particle and free space light. In the simulations of Figure 4 the gold nano-antenna is deposited on a bare dielectric membrane (with no metallic aperture) and the measured electron-light coupling results from the combined influence of the membrane and the gold nano-antenna. Neglecting the mutual influence of the membrane and nano-antenna, the electron-light coupling can be written as :

$$g_{tot} = \frac{e}{2\hbar\omega} \int dz \left[E_z^{mem}(z) + E_z^{ant}(z) \right] e^{-\imath\omega z/v} \tag{3}$$

in which $E_z^{mem}(z)$ (resp. $E_z^{ant}(z)$) is the z-component of the electric field scattered by the dielectric membrane (resp. the antenna). Equation (3) shows that the variations of the electron-light coupling originate from the interference between the optical response of the membrane and the antenna. In the PINEM experiments, the electric field radiated by the edges of the metallic aperture yields a supplementary term that adds up to the electric field scattered by the nanostructure itself and to the electric field reflected/transmitted by the membrane. This additional contribution is excited for p-polarized tilted illumination yielding a field component along the electron trajectory that can efficiently couple with the moving charge. We discuss more in details in the supplementary information the relative magnitude of the contribution of the reflection on the membrane and scattering from the aperture edge as well as a comparison of different membrane material. The experimental and theoretical results of Figure 4 reveal the interferences in the near-field of gold nano-antennas but similar interference effect should be visible in the far-field of a nano-scatterer.

To address this point, we simulated PINEM experiments on individual nano-scatterers deposited on a membrane and illuminated by a tilted plane-wave ($\theta_i = 35°$). The nano-scatterers were chosen high enough so that the tilted illumination yields an out-of-plane dipole capable of radiating electric fields with z-components of magnitude large enough to

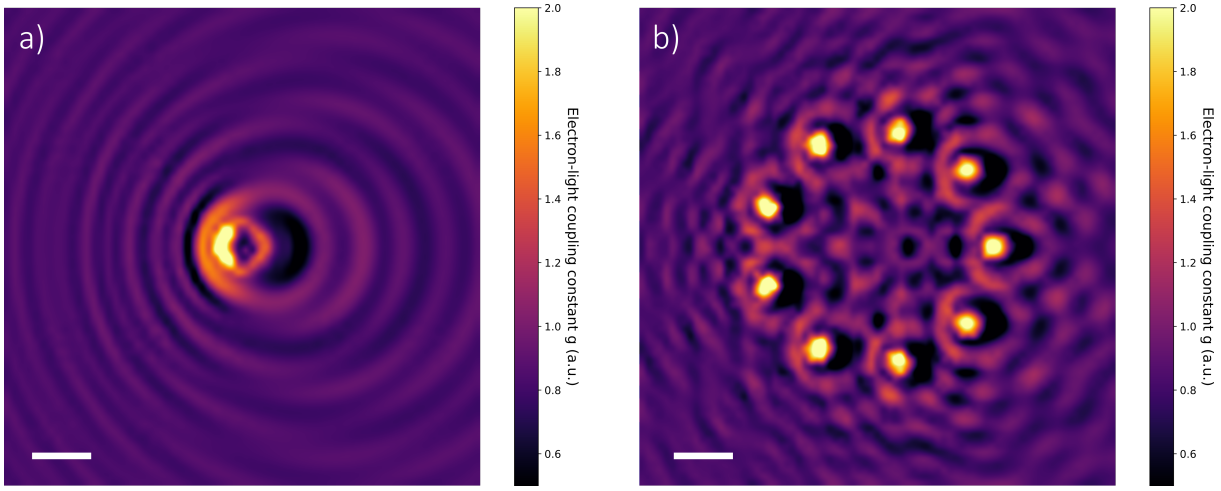

Fig. 5: (Color Online) a) PINEM map computed on a 2μm $\times$ 2μm centered on a gold disc (R = 150 nm, H = 300 nm) on a silicon nitride substrate. b) PINEM map computed on an optical corral composed of 10 identical gold nanodiscs (R = 50 nm, H = 300 nm) on a silicon nitride substrate. Scale bar = 500 nm

interfere efficiently with the incident wave. Figure 5-a displays the results in the case of a single gold nanodisc. The electron-light coupling strength displays spatial modulations reminiscent of the Doppler effect arising from the interference between the tilted incident plane wave and the secondary wave scattered by the excited metallic nano-object. We provide in supplementary information additional data computed for both s-polarized and p-polarized tilted optical excitation which confirm that the observed interferences are obtained only when the incoming electric field has a non-zero out-of-plane component, i.e for p-polarized excitation. The interferences obtained here between the scattering from the nanodiscs and the reflection from the dielectric substrate are connected to the results of[22] where the interferences between the surface plasmon polariton field propagating away from an optically excited nano-hole and the reflection from the sample were reported. Contrary to the case of Figure 4, these interferences are also visible in the far-field region of the antenna i.e at distances from the antenna much larger than the wavelength of the incident wave. It is the dielectric contrast at the membrane surface which allows the coupling between the electron and the electromagnetic field radiated by the antenna. As illustrated in Figure 5-b, when more nanostructures are considered, the spatial modulation of the electron-light coupling re-

sults from the interference between (i) the incident wave, (ii) the waves reflected/transmitted by the substrate and (iii) the different waves scattered by the nanostructures.

In the case of PINEM performed using a normally incident illumination, the spatial distribution of the electron-light coupling resembles closely the topography of the ~~amplitude of~~ the z-component of the total electric field. Our study shows that a tilted illumination is associated with a significant contribution from the substrate to the electron-light coupling that yields more complex modulations of the inelastic interaction probability due to interference effects. Such interference effects could be exploited to gain access to the phase of the different contributions to the total electric field. However, this would require careful electrodynamical simulation to take into account the different contributions to the electromagnetic field probed by the moving electron. As shown in the expression of g_{mem} provided in Eq. (1), the amplitude and phase of the contribution of the dielectric membrane to the electron/light coupling is highly sensitive to the dielectric constant, membrane thickness and geometrical parameters of the interaction. The interferences between the scattering from different nano-objects or with an aperture edge will also be very sensitive to the geometrical arrangement. Finally, the proximity of the studied nano-object with the substrate may alter the measured optical response. The configuration in which the fast electron interacts sequentially with electromagnetic fields in two different locations is demanding from the experimental point of view but should be privileged for phase-resolved measurements for two reasons[14,31]. First, a proper choice of the experimental geometry allows to exactly compensate the difference in phase velocities of the fast electron and the electromagnetic wave so that each part of the electron beam on the membrane interacts with the same optical phase providing a constant reference electron-light coupling constant throughout the studied nanostructure[14,18,31]. Second, this configuration offers the possibility of changing the separation between the two interaction regions and therefore the phase difference between the two interfering contributions. The interference effects studied in this work must however be taken into account whenever several nano-objects are probed simultaneously or with an optical excitation away

from normal incidence.

Conclusions

In conclusion we have studied both experimentally and theoretically the electron-light coupling in apertures and nanostructures fabricated on a dielectric membrane. Our results show that the scattering from the aperture edges as well as the electric field reflected or transmitted by the dielectric membrane illuminated by a tilted plane wave contribute significantly to the modulation of the electron-light coupling strength measured in PINEM. This contribution from the membrane interferes with the electric field scattered by nanostructures fabricated on the membrane and alters the electron-light coupling both in the near-field and far-field region. Whereas the analysis of the experimental results in this configuration requires a careful analysis and comparison with electrodynamical simulations, these interference effects could be exploited to map the phase of the electric fields scattered by complex nanostructures.

Acknowledgement

This project has been funded in part by the European Union's Horizon 2020 research and innovation program under Grant Agreement Nos. 823717 (ESTEEM3). This project has been funded in part by the ANR under Grant Agreement No. ANR-19-CE30-0008 ECHOMELO and Grant Agreement No. ANR-20-CE30-0033 QUENOT. This work was supported by Programme Investissements d'Avenir under the Program ANR-11-IDEX-0002-02, reference ANR-10-LABX-0037-NEXT (MUSE grant) and EUR grant NanoX ANR-17-EURE-0009 (LifeTEM). This work was supported by the Toulouse HPC CALMIP (grant P08122). All authors declare no competing interest.

Supporting Information Available

Sample fabrication; Electron energy gain experiments and data processing, PINEM experiments: complementary data; PINEM theory in a nutshell, Energy exchange induced by a perfect mirror; Case of an aperture membrane, Diffracting the edge of a metallic film; Electrodynamical simulations using the Green Dyadic Methods; Contributions of scattering by the metallic film edge and dielectric membrane to the modulations of the electron light coupling constant.

References

(1) Zewail, A. H.; Thomas, J. M. 4d Electron Microscopy: Imaging in Space and Time; Imperial College Press, 2009.

(2) Arbouet, A.; Caruso, G. M.; Houdellier, F. In Advances in Imaging and Electron Physics; Hawkes, P. W., Ed.; Advances in Imaging and Electron Physics; Elsevier, 2018; Vol. 207; pp 1–72.

(3) Feist, A.; Storeck, G.; Schäfer, S.; Ropers, C. Structural dynamics probed by high-coherence electron pulses. MRS Bulletin **2018**, 43, 504–511.

(4) Harvey, T. R.; Rubiano Da Silva, N.; Gaida, J. H.; Möller, M.; Feist, A.; Schäfer, S.; Ropers, C. Ultrafast electron microscopy for probing magnetic dynamics. MRS Bulletin **2021**, 46, 711–719.

(5) Adhikari, A.; Eliason, J. K.; Sun, J.; Bose, R.; Flannigan, D. J.; Mohammed, O. F. Four-Dimensional Ultrafast Electron Microscopy: Insights into an Emerging Technique. ACS Applied Materials & Interfaces **2017**, 9, 3–16, Publisher: American Chemical Society.

(6) Aseyev, S. A.; Ryabov, E. A.; Mironov, B. N.; Ischenko, A. A. The Development of

Ultrafast Electron Microscopy. Crystals **2020**, 10, 452, Number: 6 Publisher: Multidisciplinary Digital Publishing Institute.

(7) Abajo, F. J. G. d.; Kociak, M. Electron energy-gain spectroscopy. New Journal of Physics **2008**, 10, 073035.

(8) Barwick, B.; Flannigan, D. J.; Zewail, A. H. Photon-induced near-field electron microscopy. Nature **2009**, 462, 902–906.

(9) Feist, A.; Echternkamp, K. E.; Schauss, J.; Yalunin, S. V.; Schafer, S.; Ropers, C. Quantum coherent optical phase modulation in an ultrafast transmission electron microscope. Nature **2015**, 521, 200–203.

(10) Park, S. T.; Zewail, A. H. Photon-induced near-field electron microscopy (PINEM): theoretical and experimental. New Journal of Physics **2010**, 12, 123028–.

(11) Yurtsever, A.; Zewail, A. H. Direct Visualization of Near-Fields in Nanoplasmonics and Nanophotonics. Nano Letters **2012**, 12, 3334–3338.

(12) Barwick, B.; Zewail, A. H. Photonics and Plasmonics in 4D Ultrafast Electron Microscopy. ACS Photonics **2015**, 2, 1391–1402.

(13) Piazza, L.; Lummen, T. T. A.; Quiñonez, E.; Murooka, Y.; Reed, B. W.; Barwick, B.; Carbone, F. Simultaneous observation of the quantization and the interference pattern of a plasmonic near-field. Nature Communications **2015**, 6, 6407.

(14) Echternkamp, K. E.; Feist, A.; Schafer, S.; Ropers, C. Ramsey-type phase control of free-electron beams. Nat Phys **2016**, 12, 1000–1004.

(15) Priebe, K. E.; Rathje, C.; Yalunin, S. V.; Hohage, T.; Feist, A.; Schäfer, S.; Ropers, C. Attosecond electron pulse trains and quantum state reconstruction in ultrafast transmission electron microscopy. Nature Photonics **2017**, 11, 793.

(16) Pomarico, E.; Madan, I.; Berruto, G.; Vanacore, G. M.; Wang, K.; Kaminer, I.; García de Abajo, F. J.; Carbone, F. meV Resolution in Laser-Assisted Energy-Filtered Transmission Electron Microscopy. ACS Photonics **2017**,

(17) Kfir, O.; Lourenço-Martins, H.; Storeck, G.; Sivis, M.; Harvey, T. R.; Kippenberg, T. J.; Feist, A.; Ropers, C. Controlling free electrons with optical whispering-gallery modes. Nature **2020**, 582, 46–49.

(18) Kirchner, F. O.; Gliserin, A.; Krausz, F.; Baum, P. Laser streaking of free electrons at 25 keV. Nature Photonics **2014**, 8, 52–57.

(19) Vanacore, G. M.; Madan, I.; Berruto, G.; Wang, K.; Pomarico, E.; Lamb, R. J.; McGrouther, D.; Kaminer, I.; Barwick, B.; García de Abajo, F. J.; Carbone, F. Attosecond coherent control of free-electron wave functions using semi-infinite light fields. Nature Communications **2018**, 9, 2694.

(20) Konečná, A.; de Abajo, F. J. G. Electron Beam Aberration Correction Using Optical Near Fields. Physical Review Letters **2020**, 125, 030801.

(21) Madan, I.; Leccese, V.; Mazur, A.; Barantani, F.; LaGrange, T.; Sapozhnik, A.; Tengdin, P. M.; Gargiulo, S.; Rotunno, E.; Olaya, J.-C.; Kaminer, I.; Grillo, V.; de Abajo, F. J. G.; Carbone, F.; Vanacore, G. M. Ultrafast Transverse Modulation of Free Electrons by Interaction with Shaped Optical Fields. ACS Photonics **2022**, Publisher: American Chemical Society.

(22) Madan, I.; Vanacore, G. M.; Pomarico, E.; Berruto, G.; Lamb, R. J.; McGrouther, D.; Lummen, T. T. A.; Latychevskaia, T.; García de Abajo, F. J.; Carbone, F. Holographic imaging of electromagnetic fields via electron-light quantum interference. Science Advances **2019**, 5, eaav8358.

(23) Houdellier, F.; Caruso, G. M.; Weber, S.; Kociak, M.; Arbouet, A. Development of

a high brightness ultrafast Transmission Electron Microscope based on a laser-driven cold field emission source. Ultramicroscopy **2018**, 186, 128–138.

(24) Caruso, G. M.; Houdellier, F.; Abeilhou, P.; Arbouet, A. Development of an ultrafast electron source based on a cold-field emission gun for ultrafast coherent TEM. Applied Physics Letters **2017**, 111, 023101.

(25) Caruso, G. M.; Houdellier, F.; Weber, S.; Kociak, M.; Arbouet, A. High brightness ultrafast transmission electron microscope based on a laser-driven cold-field emission source: principle and applications. Advances in Physics: X **2019**, 4, 1660214.

(26) Born, M.; Wolf, E. Principles of Optics: Electromagnetic Theory of Propagation, Interference and Diffraction of Light (7th Edition), 7th ed.; Cambridge University Press, 1999.

(27) Martin, O. J. F.; Girard, C.; Dereux, A. Generalized Field Propagator for Electromagnetic Scattering and Light Confinement. Phys. Rev. Lett. **1995**, 74, 526–.

(28) Girard, C. Near fields in nanostructures. Reports on Progress in Physics **2005**, 68, 1883–1933.

(29) Wiecha, P. R.; Majorel, C.; Arbouet, A.; Patoux, A.; Brûlé, Y.; Colas des Francs, G.; Girard, C. "pyGDM" - new functionalities and major improvements to the python toolkit for nano-optics full-field simulations. Computer Physics Communications **2022**, 270, 108142.

(30) Arbouet, A.; Mlayah, A.; Girard, C.; Colas des Francs, G. Electron energy losses and cathodoluminescence from complex plasmonic nanostructures: spectra, maps and radiation patterns from a generalized field propagator. New Journal of Physics **2014**, 16, 113012–.

(31) Gaida, J. H.; Lourenço-Martins, H.; Sivis, M.; Rittmann, T.; Feist, A.; de Abajo, F. J. G.; Ropers, C. Attosecond electron microscopy by free-electron homodyne detection. 2023.